Journal of Inorganic Biochemistry 216 (2021) 111339

Contents lists available at ScienceDirect

Journal of Inorganic Biochemistry

journal homepage: www.elsevier.com/locate/jinorgbio

Enantiomeric selectivity of ruthenium (II) chiral complexes with antitumor activity, *in vitro* and *in vivo*

Weiwei Zhang [a,c], Yu Sun [a], Jingyuan Wang [a], Xiaoyuan Ding [a], Endong Yang [a], Lisandra L. Martin [b,*], Dongdong Sun [a,*]

[a] School of Life Sciences, Anhui Agricultural University, Hefei 230036, China
[b] School of Chemistry, Monash University, Clayton 3800, Victoria, Australia
[c] School of Biochemical Engineering, Anhui Polytechnic University, Beijing Middle Road, 241000 Wuhu, Anhui, China

ARTICLE INFO

Keywords:
Chiral complexes
Ruthenium
Fluorescent probes
AIE
Anticancer

ABSTRACT

Different enantiomers of chiral drugs show distinctive activities. Here, a pair of chiral ruthenium Λ-[Ru(phen)$_2$(TPEPIP)]$^{2+}$ (Λ-Ru), and Δ-[Ru(phen)$_2$(TPEPIP)]$^{2+}$ (Δ-Ru) (phen = 1,10-phenanthroline; TPEPIP = 2-(4′-(1,2,2-triphenylvinyl)-[1,1′-biphenyl]-4-yl)-1H-imidazo[4,5-f][1,10]phenanthroline) compounds have been prepared and characterized. Both have aggregation-induced emission characteristics, although Λ-Ru exhibits much higher activity, towards duplex DNA extracted from SGC-7901 cancer cells. In vitro experiments demonstrate that both Λ-Ru and Δ-Ru can induce the apoptosis of tumor cells with Λ-Ru showing greater activity than Δ-Ru. Λ-Ru aggregates in the cell nucleus of SGC-7901 within 5 h which shows that nucleic acids may be the effective target of Λ-Ru. In vivo experiments with nude mice showed that Λ-Ru can inhibit the growth and proliferation of a tumor, in tumor-bearing mice as well as targeting the tumor site, as demonstrated by fluorescence. These results demonstrate the dual-function of Λ-Ru, which could be used for real-time visualization of a chemotherapeutic agent.

1. Introduction

Cancer is a leading cause of mortality, with predictions of more than 21 million cases by 2030. According to the World Health Organization, in 2015, the number of deaths caused by cancer was 8.8 million, with nearly one in six deaths globally being attributed to cancer [1,2]. There is also an economic loss due to deaths from cancer, which is increasing concomitantly. Some of the recent approaches to combat this proliferation of cancers, have been reviewed by Chen et al. [3], who highlighted the use of intelligent molecules as theranostics. These intelligent molecules combine cancer diagnostics, especially those developed for imaging, with therapeutic activity required for cancer treatment [4–6]. Novel fluorescent molecules, which can target cancer cells at the molecular level, have also attracted significant interest. However, these molecules have one major drawback which is quenching of the fluorescence due to aggregation [7–9]. There are numerous examples of fluorescent organic polymers that are highly emissive in dilute solution but become weakly luminescent as they concentrate and form aggregates [10]. Activatable fluorophores with aggregation-induced emission (AIE) activity have been successful is overcoming this limitation and are used to detect binding events and have been especially successful in biosensing and bioimaging applications [11,12].

The asymmetric synthesis of chiral secondary alcohols, which play an important role as intermediates in organic chemistry, is a stimulating subject. In previous studies, ruthenium complexes exhibited good antitumor activities and prominent DNA-binding properties [13–15]. Previously, Sun et al. have reported that Ru-SeNPs (ruthenium-modified selenium nanoparticles) inhibit angiogenesis suggesting possible

Abbreviations: AIE, aggregation-induced emission; ATCC, American Type Culture Collection; BDTPE, 4′-(1,2,2-triphenylvinyl)-[1,1′-biphenyl]-4-carbaldehyde phenanthroline; bpy, 2,2′-bipyridine; CD, circular dichroism; CLSM, confocal laser scanning microscopy; DAPI, 4′,6-diamidino-2-phenylindole; dppf, 1,1′-bis(diphenylphosphino)ferrocene; H&E, hematoxylin and eosin (stain); MRI, magnetic resonance imaging; MTT, thiazolyl blue tetrazolium bromide; phen, 1,10-phenanthroline; PI, propidium iodide; RTCA, real-time cellular analysis; Ru-SeNPs, ruthenium-modified selenium nanoparticle; SEM, scanning electron microscopy; TEM, transmission electron microscopy; THF, Tetrahydrofuran; TPE, tetraphenylethene; TPE-Br, (2-(4-Bromophenyl)ethene-1,1,2-triyl)tribenzene; TPEPIP, 2-(4′-(1,2,2-triphenylvinyl)-[1,1′-biphenyl]-4-yl)-1H-imidazo[4,5-f][1,10]; TUNEL, (terminal deoxynucleotidyl transferase-mediated dUTP nick-end labeling).

* Corresponding authors.
E-mail addresses: Lisa.Martin@monash.edu (L.L. Martin), sunddwj@126.com (D. Sun).

https://doi.org/10.1016/j.jinorgbio.2020.111339
Received 19 July 2020; Received in revised form 12 December 2020; Accepted 13 December 2020
Available online 28 December 2020
0162-0134/

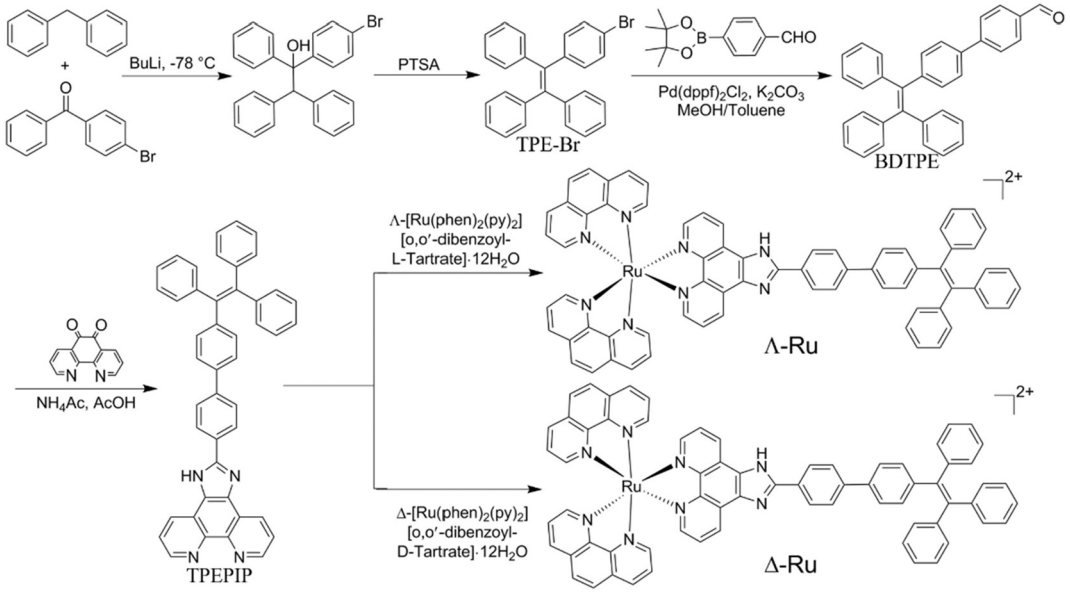

Scheme 1. The sequence of reactions used to prepare the Λ-Ru and Δ-Ru complexes, as described in ref. [29].

applications as viable drug candidates for anti-angiogenesis and anti-cancer therapies [16]. Here we employ Ru(II) complexes with poly-pyridyl ligands, which provide a combination of modular construction with a rigid chiral, and 3D spatial structures. The rich photophysical properties and DNA-binding capabilities provide significant improvements compared with traditional drugs. Independently, there have been reports that Ru(II) dipyridophenazine complexes (Puckett et al. [17]) and examples of arene Ru(II) complexes (Wu et al. [15]) that have low toxicity and were readily absorbed and rapidly excreted in vivo. Thus, these ruthenium complexes offer enormous potential with applications for dual imaging in antitumor treatment [18–20].

In the current study, we report on the properties of two, dual-function ruthenium complexes that achieve real-time visualization (imaging) and therapeutic activity, towards tumor cells. We modified one of the three phen (1,10-phenanthroline) ligands in a ruthenium complex with a tetraphenylethene (TPE) moiety, because AIE is usually retained after chemical modification [21–24]. Importantly, previous studies have shown that ruthenium complexes can combine with the tumor cell nuclei of target (tumor) cells [25–27]. Thus, the target of the tumor cell is also thought to be the nucleus, with the chiral Λ-Ru and Δ-Ru complexes binding to duplex DNA in the tumor cells. Thus, we expected AIE behavior from the ruthenium complexes to provide fluorescence imaging of the tumor cells. This study provides a new insight into the application of dual-function, AIE theranostics for targeted bio-imaging and therapy using chiral ruthenium complexes.

2. Experimental

2.1. Materials and methods

The reagents used in the synthesis were purchased from Sigma-Aldrich Chemical Co. (USA). All solvents for synthesis were of reagent grade and were used as received. For spectroscopic studies spectroscopy-grade solvents were used.

2.2. Synthesis and general characterization of the complexes

(2-(4-Bromophenyl)ethene-1,1,2-triyl)tribenzene (TPE-Br) was synthesized according to the literature [28]. 1,10-phenanthroline-5,6-dione, Λ-[Ru(phen)$_2$(py)$_2$][O,O′-dibenzoyl-D-tartrate]•12H$_2$O, and Δ-[Ru(phen)$_2$(py)$_2$][O,O′-dibenzoyl-L-tartrate]•12H$_2$O (py = pyridine) were synthesized in our previous study [29]. The synthetic strategy for the preparation of Λ-Ru and Δ-Ru is presented in Scheme 1.

2.3. Preparation of 4′-(1,2,2-triphenylvinyl)-[1,1′-biphenyl]-4-carbaldehyde (BDTPE)

[Pd(dppf)]Cl$_2$ (0.06 mmol) (dppf = 1,1′-bis(diphenylphosphino) ferrocene) was added to a well-degassed solution of 4-(4,4,5,5-tetramethyl-1,3,2-dioxaborolan-2-yl)benzaldehyde (1.8 mmol), (2-(4-bromophenyl)ethene-1,1,2-triyl)tribenzene (1.2 mmol), and K_2CO_3 (6.1 mmol) in a mixture of methanol (12.5 mL) and toluene (12.5 mL). The mixture was stirred at 75 °C for 18 h under argon atmosphere. The mixture was evaporated to dryness and taken up with CH_2Cl_2. The organic layer was washed with H_2O, dried over $NaSO_4$, filtered, and evaporated to dryness, producing a light-yellow powder in 88% yield. Elemental analysis: calculated for $C_{33}H_{24}O$: C 90.83, H 5.47; found: C 90.64, H 5.47%.

2.4. Preparation of 2-(4′-(1,2,2-triphenylvinyl)-[1,1′-biphenyl]-4-yl)-1H-imidazo[4,5-f][1,10] phenanthroline (TPEPIP)

4′-(1,2,2-Triphenylvinyl)-[1,1′-biphenyl]-4-carbaldehyde (0.4 mmol), 1,10-phenanthroline-5,6-dione (0.4 mmol), and $NH_4(CH_3CO_2)$ (8 mmol) were stirred in CH_3CO_2H (5 mL) at 110 °C for 18 h under argon atmosphere. The mixture was then poured into a large amount of water, the pH adjusted 7 and left overnight. The resulting solid was filtered and washed with ethanol and then placed under high-vacuum pressure overnight. 2-(4′-(1,2,2-Triphenylvinyl)-[1,1′-biphenyl]-4-yl)-1H-imidazo[4,5-f][1,10] phenanthroline was obtained as a slightly pink solid in 67% yield. Elemental analysis: calculated for $C_{45}H_{30}N_4$: C 86.23, H 4.82, N 8.94; found: C 86.11, H 4.80, N 8.90%. (^{1}H NMR (600 MHz, DMSO-d_6) δ 13.78 (s, 1H), 9.03 (s, 2H), 8.93 (d, J = 7.9 Hz, 2H), 8.33 (d, J = 8.0 Hz, 2H), 7.86 (dd, J = 26.3, 7.8 Hz, 4H), 7.60 (d, J = 7.8 Hz, 2H), 7.13 (ddt, J = 24.0, 16.9, 8.7 Hz, 12H), 7.03 (dd, J = 15.3, 7.7 Hz, 5H). ESI-MS (in CH_3OH, m/z):1087.2 [M]-) (Supporting Information (SI) Fig. S1 ESI†).

2.5. Preparation of Λ-Ru

TPEPIP (0.3 mmol) and Λ-[Ru(phen)$_2$(py)$_2$][O,O′-dibenzoyl-L-tartrate]•12H$_2$O (0.2 mmol) were mixed in ethylene glycol (20 mL) and

refluxed for 8 h under an argon atmosphere. (Λ-[Ru(phen)$_2$(py)$_2$][O,O′-dibenzoyl-L-tartrate]•12H$_2$O was purchased from Sigma-Aldrich Chemical Co., USA). The cooled reaction mixture was diluted with water (50 mL) and filtered to remove solid impurities, and then saturated ammonium perchlorate aqueous solution was added to the filtrate. A deep red solid was collected and dried in a small amount of water in a vacuum and then purified by column chromatography (Al_2O_3, acetonitrile/toluene 1:1), giving a yield of 68% of a dark red powder. Elemental analysis: calculated for Λ-Ru ($C_{69}H_{46}N_8Cl_2O_8Ru.2H_2O$): C 60.96, H 3.70, N 8.24; found: C 60.81, H 3.68, N 8.21%. (^{1}H NMR (600 MHz, DMSO-d_6) δ 13.81 (s, 1H), 9.05 (d, J = 8.3 Hz, 4H), 9.01 (d, J = 4.3 Hz, 2H), 8.92 (t, J = 7.7 Hz, 2H), 8.76 (d, J = 8.2 Hz, 8H), 8.37 (s, 8H), 8.33 (dd, J = 15.0, 8.0 Hz, 7H), 8.11 (d, J = 5.2 Hz, 4H), 8.06 (d, J = 5.2 Hz, 4H), 7.98 (d, J = 5.3 Hz, 4H), 7.88 (t, J = 6.4 Hz, 7H), 7.75 (dd, J = 8.3, 5.4 Hz, 9H), 7.59 (dd, J = 11.9, 8.0 Hz, 7H). ESI-MS (in CH_3OH, m/z):1087.2 [M]-) (SI, Fig. S2 ESI†).

2.6. Preparation of Δ-Ru

A mixture of TPEPIP (0.3 mmol) and Δ-[Ru(phen)$_2$(py)$_2$][O,O′-dibenzoyl-D-tartrate]•12H$_2$O (0.2 mmol) in ethylene glycol (20 mL) was refluxed for 8 h under argon atmosphere. (Δ-[Ru(phen)$_2$(py)$_2$][O,O′-dibenzoyl-D-tartrate]•12H$_2$O were purchased from Sigma-Aldrich Chemical Co., USA). The cooled reaction mixture was diluted with water (50 mL). A saturated aqueous ammonium perchlorate solution was added, mixed vigorously, and filtered. A dark red solid was collected, washed with small amounts of water, dried under vacuum, and purified by column chromatography (Al_2O_3, acetonitrile/toluene 1:1), producing a dark red powder in 71% yield. Elemental analysis: calculated for Δ-Ru ($C_{69}H_{46}N_8Cl_2O_8Ru.2H_2O$): C 60.96, H 3.70, N 8.24; found: C 61.11, H 3.69, N 8.26%. (^{1}H NMR (600 MHz, DMSO-d_6) δ 9.04 (s, 2H), 8.90 (s, 1H), 8.75 (d, J = 8.1 Hz, 6H), 8.37 (s, 6H), 8.32 (s, 2H), 8.11 (s, 3H), 8.06 (s, 4H), 7.97 (t, J = 6.8 Hz, 4H), 7.84 (s, 3H), 7.75 (s, 7H), 7.54 (s, 2H), 7.44 (t, J = 7.4 Hz, 2H), 7.14 (dt, J = 16.8, 8.6 Hz, 26H), 7.08 (s, 7H), 7.06–6.95 (m, 20H). ESI-MS (in CH_3OH, m/z):1087.2 [M]-) (SI, Fig. S3 ESI†).

2.7. Characterization

The UV–visible absorption spectra were registered using ultraviolet-visible spectroscopy (UV–vis, S-3100 photodiode array, Scinco Co., Korea). CD spectra were collected at 37 °C with a JASCO J-810 spectropolarimeter using a 1 mm path length quartz cell. Λ-Ru and Δ-Ru (1 μM) was added in 0.5 mL DMSO and then diluted to obtain a stock solution (buffered with Tris-HCl, TRIS is trisaminomethane, 10 mM, pH 7.4). Duplex DNA (SGC-7901 cell nucleus material) was extracted from the nucleus pellet using a cell DNA extraction Kit (Sangon Biotech, Shanghai, China). DNA stock solutions were prepared and diluted with the Tris-HCl buffer (pH = 8).

2.8. Cell cultures

HeLa, HepG-2, SGC-7901, A549, and MRC-5 cell lines were purchased from ATCC (American Type Culture Collection) and maintained in RPMI (Roswell Park Memorial Institute) with 10% fetal bovine serum at 37 °C and under an atmosphere with 5% CO_2.

2.9. Cytotoxicity assays

The cells were seeded in 96-well plates at 37 °C for 12 h. All cultured cells grew against the side of the well overnight, and different compounds at varying concentrations were added into the plate and then cell culture continued for 12 h. Cell viabilities were measured using a standard MTT (3-(4,5-dimethylthiazol-2-yl)-2,5-diphenyltetrazolium bromide) colorimetric assay. These experiments were performed strictly in the dark.

2.10. Real-time cell analysis

The cell proliferation was analyzed by real-time cellular analysis (RTCA), using a multielectrode array-based RTCA system (ACEA Biosciences, Inc., San Diego, CA, USA). Cells were plated at a density of 5000/well with a fresh medium to a final volume of 200 μL. After cell culture for 12 h, the medium was removed, and a fresh medium with different concentrations of Λ-Ru and Δ-Ru (2.5 μM, 5 μM, and 10 μM) was added. Cells were incubated at 37 °C and 5% CO_2 in the RTCA system cradle. The signals were recorded every 10 min for 60 h. The experiment was performed strictly in the dark.

2.11. Fluorescence microscopic observation (live/dead)

For the fluorescence microscopic observations, SGC-7901 cells (2.0×10^4 cells/well) were placed in 48-well plates overnight. The cells were incubated with different concentrations of Λ-Ru and Δ-Ru (2.5 μM, 5 μM, and 10 μM) for 12 h. The cells were co-stained using the LIVE/DEAD Kit (Sigma-Aldrich Chemical) for 30 min under dark conditions. After removing the culture medium, calcein-AM (10 ng/mL, 1 mL) and Propidium iodide (PI) (10 ng/mL, 1 mL) were mixed and added into the wells of the culture dishes, which were then incubated for 30 min in the dark. Then, all dishes were washed three times with phosphate buffered saline solution (PBS) and observed by confocal laser scanning microscopy (CLSM). The experiment was performed strictly in the dark.

2.12. Apoptotic cell death analysis

SGC-7901 cells were grown in 6-well plates overnight at 37 °C and 5% CO_2. The cells were then treated with Λ-Ru and Δ-Ru (2.5 μM, 5 μM, and 10 μM) and the culture continued for 12 h. The blank group was PBS. After treatment, the cells were collected and washed twice with PBS. The cells were collected and stained with PI and Annexin V, and then analyzed by a CytoFLEX flow cytometer (Beckman Coulter). Annexin V could detect early apoptotic cells due to being bound to the exposed phosphatidylserine. PI labeling was used to stain the late apoptotic cells. The experiment was performed strictly in the dark. (PI, Ex = 535 nm, and Em = 615 nm. Annexin V-FITC, Ex = 488 nm, and Em = 525 nm).

2.13. Membrane integrity and wall destruction studies

Germ-free silicon wafers were placed into six-well plates. The SGC-7901 cells were grown on the surface of silicon wafers overnight at 37 °C and 5% CO_2. The cells were subjected to the same treatment with different concentrations of Λ-Ru and Δ-Ru (2.5 μM, 5 μM, and 10 μM) for 12 h. The cells cultured without a complex were used as the blank group. The cells with the silicon wafers were dehydrated with a series of ethanol concentrations after they were fixed with 2.5% glutaraldehyde overnight. The cells were then dried with a critical point drier and observed by scanning electron microscope (SEM) (S-4800, Hitachi, Japan) for the study of membrane intensity. The experiment was performed strictly in the dark.

For the study on wall destruction, the SGC-7901 cells were grown in six-well plates overnight at 37 °C and 5% CO_2. The cells cultured without a complex were used as the blank group. After being subjected to the same treatment with different concentrations of Λ-Ru and Δ-Ru

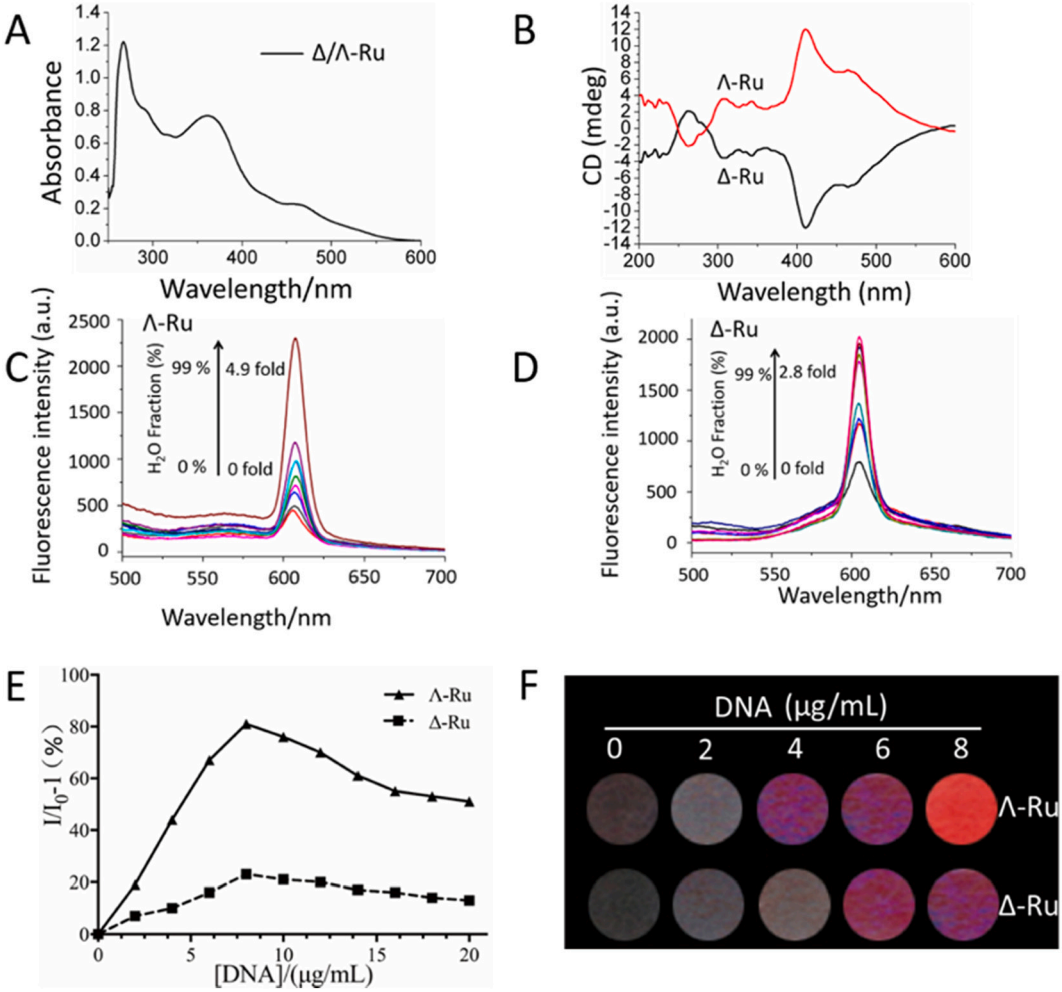

Fig. 1. (A) UV − vis absorption spectrum of Λ-Ru and Δ-Ru in THF. (B) Circular dichroism (CD) spectroscopy of Λ-Ru and Δ-Ru in THF. (C) Fluorescence spectra of Λ-Ru (10 μM), with increasing H_2O fraction was from 0% to 99% (or 0 to 4.9-fold). (D) Fluorescence spectra of Δ-Ru (10 μM), with increasing H_2O fraction from 0% to 99% (or 0 to 4.9-fold). (E) Variation of the relative fluorescence intensity (I/I_0-1) of Λ-Ru and Δ-Ru with increasing duplex DNA concentration; I is the fluorescence intensity of Λ-Ru or Δ-Ru, and I_0 is the fluorescence intensity without duplex DNA present; λex = 300 nm. (F) Images of 1 μM Λ-Ru (1 μM) and Δ-Ru (1 μM) with increasing concentrations of duplex DNA. (left to right concentrations are 0, 2, 4, 6, and 8 μg/mL).

(2.5 μM, 5 μM, and 10 μM) for 12 h, the cells were treated with Trypsin-EDTA solution 0.25%. All cells (including the floating cells in the medium) were collected with 1000 r/min for 5 min. The cells were ultimately treated with a series of processing steps to be mounted on copper grids and observed by transmission electron microscopy (TEM) (HT-7700, Hitachi, Japan). The experiment was performed strictly in the dark.

2.14. Real-time cell fluorescence imaging

For real-time cell fluorescence imaging, SGC-7901 cells were seeded in 48-well plates at 37 °C and grown for 12 h. The cells were then treated with Λ-Ru and Δ-Ru (5 μM). After incubation for different time periods, fluorescence and normal images were taken under a 60 × oil-immersion objective by using the real-time cell fluorescence imaging system. For Λ-Ru and Δ-Ru, the excitation filter was 300 nm, and the emission filter was 630–760 nm. The experiment was performed strictly in the dark.

2.15. Animal model and in vivo chemotherapy

BALB/c male nude mice (~25 g) were purchased from the Model Animal Research Center of Nanjing University and bred in a specific pathogen free environment. All animals received care in compliance with the guidelines outlined in the Guide for the Care and Use of Laboratory Animals. All animal experiments were carried out according to the protocols approved by Anhui Agricultural University Laboratory Animal Center (Permit Number: SYXK 2016-007). Tumor models were established by subcutaneous injection of cell suspension (SGC-7901 cells, 100 μL, 1 × 10 [6]/mL) into the shoulder of the nude mice. When the tumor volume reached about 100 mm^3, the mice were randomized into 3 groups ($n = 6$ per group): the untreated control Ru group, 2.5 μM group, and 5 μM Ru group. Dosing solutions were administered via intravenous injection every 3 days during the experiment.

To determine the tumor volume, a vernier caliper was used to find the maximum longitudinal diameter (length) and maximum transverse diameter (width) of each tumor, and the tumor volume was calculated using length × width [2] × 0.5. At the end of the experimental period, with consecutive anesthetizations using 2% isoflurane in oxygen,

Magnetic resonance imaging (MRI) was used to obtain images of the whole mice and tumor tissue with SGC-7901 xenograft subcutaneous models with a 3.0-TMR scanner (General Electric, Milwaukee, WI, USA). The mice were sacrificed, and the tumor tissues removed, rinsed with physiological saline, and weighed. The tumor tissues were finely sliced using a cryotome. The frozen tumor sections were then stained with TUNEL (terminal deoxynucleotidyl transferase-mediated dUTP nick-end labeling) and DAPI (4′,6-diamidino-2-phenylindole) and then observed by fluorescence microscopy.

2.16. Toxicity assay in vivo

To evaluate the toxicity of Λ-Ru, the mice were sacrificed after 14 days. The PBS treated mice were used as the blank group. The mice were treated with different concentrations of Λ-Ru (2.5 μM, 5 μM, and 10 μM). The important organs (liver, spleen, kidneys, heart, and lungs) of the mice were collected and stained with hematoxylin and eosin (H&E). The body weight and survival rate were also measured during treatment time.

2.17. In vivo fluorescence imaging

Male nude SGC-7901 subcutaneous models were administered intravenous tail injections with Λ-Ru (5 μM). Fluorescence signal photographs (640 ± 20 nm) were taken at different time points. The fluorescence images of the whole mice were taken after injection using the IVIS spectrum in vivo fluorescence imaging system (Calipaer Perkin Elmer).

3. Results and discussion

3.1. Characterization of Λ-Ru and Δ-Ru

The spectroscopic characterization of Λ-Ru and Δ-Ru were evaluated as shown in Fig. 1. Λ-Ru and Δ-Ru are soluble in polar solvents, such as DMSO and Tetrahydrofuran (THF), but exhibit low solubility in water. We first measured their Ultraviolet–visible (UV–vis) absorption spectra, where Λ-Ru and Δ-Ru showed identical absorption characteristics (Fig. 1A). In the present study, to further determine the factors that govern the optical activity of a chiral complex, we investigated circular dichroism (CD) spectral responses of Λ-Ru and Δ-Ru. The CD spectra are shown in Fig. 1B for the two complexes where a clear mirror image relationship between the Λ-Ru and Δ-Ru was exhibited. These data confirmed that Λ-Ru and Δ-Ru have the correct chirality. Mixtures of DMSO with varying amounts of water were used to check emission activity. Fig. 1C and D show the occurrence of AIE observed for Λ-Ru and Δ-Ru in dilute THF solution, where both exhibit low emission intensities. With an increase in the percentage of water, AIE gradually increases, and where the amount of water exceeds 90%, AIE quickly rises. The maximum emission intensity of Λ-Ru is observed at 608 nm, and that of Δ-Ru was observed at 608 nm. These characterization data confirmed that Λ-Ru and Δ-Ru were chiral compounds, and that both these chiral compounds had AIE properties.

3.2. Fluorescence titration of DNA

Λ-Ru and Δ-Ru are positively charged molecules, while duplex DNA carries a large number of negative phosphate anions. Λ-Ru and Δ-Ru molecules can attract duplex DNA [30]. To confirm the interaction, fluorescence assays were performed by adding the duplex DNA to a stock solution containing 1 mM Λ-Ru or Δ-Ru. The duplex DNA concentration was calibrated by UV–visible spectroscopy prior to the titration experiments. Fluorescence intensity was correlated with the concentration by using I/I_0-1, where I_0 and I are the peaks of fluorescence intensities with and without DNA, respectively. Fig. 1E and F show linear growth when the duplex DNA concentration increases within a certain range. The fluorescence enhancement of Λ-Ru is more intense than that of Δ-Ru, indicating high-contrast fluorescence and a high combination rate before and after duplex DNA addition. This observation indicates that Λ-Ru can aggregate more on the duplex DNA, compared with Δ-Ru. When the duplex DNA concentration exceeds the threshold, the Λ-Ru and Δ-Ru molecules may find more binding sites on different duplex DNA chains, thereby increasing the molecular aggregation and assembly of Λ-Ru or Δ-Ru with DNA. Thus, the fluorescence intensity of the system slowly decreases. To provide additional evidence for the enantiomeric selectivity of both complexes towards DNA, we undertook viscosity measurements for both Λ-Ru and Δ-Ru complexes using SGC-7901 DNA. Hydrodynamic measurements, such as viscosity, are regarded as the most critical test of binding between two entities in solution, especially in the absence of X-ray crystallographic data. Fig. S4 (SI) shows the changes in the relative viscosity of SGC-7901 DNA in the presence of ethidium bromide (EB), Λ-Ru or Δ-Ru. EB is a well-known intercalator of DNA and these results show the expected increase in relative viscosity due to an increase in length of the DNA double helix through intercalation. Thus, both the Λ-Ru and Δ-Ru complexes appear to bind to SGC-7901 DNA, similarly to EB. Of the two complexes, clearly Λ-Ru binds more effectively and Δ-Ru less well to the SGC-7901 DNA. However, taken together, it appears that both Ru complexes bind DNA in a similar manner to EB; thus, we assume that they intercalate between the base-pairs of DNA helices.

Table 1
IC_{50} of different compounds in various cancer cells compared to an MRC-5 control cell line.

Complex	IC_{50} (μM)				
	HeLa	HepG-2	SGC-7901	A549	MRC-5
Λ-Ru	26.8 ± 3.6	20.4 ± 1.7	7.6 ± 1.5	25.6 ± 2.8	51.1 ± 3.1
Δ-Ru	39.6 ± 3.4	70.2 ± 9.3	15.1 ± 1.3	26.1 ± 1.3	36.3 ± 2.5
TPE-Br	36.7 ± 1.6	49.2 ± 5.8	33.2 ± 4.5	39.9 ± 2.9	42.3 ± 2.7
BDTPE	41.5 ± 3.2	43.8 ± 2.5	48.1 ± 2.9	34.2 ± 3.8	55.7 ± 1.9
TPEPIP	46.3 ± 5.2	41.7 ± 2.9	43.9 ± 3.3	38.8 ± 4.4	44.7 ± 2.9
Cisplatin	15.2 ± 1.5	21.4 ± 1.1	18.3 ± 1.3	22.6 ± 1.8	36.8 ± 3.7

Data are average values of at least three replicates.

3.3. Anti-tumor activity of Λ-Ru and Δ-Ru

Numerous studies have indicated that ruthenium complexes exhibit higher antitumor activity as well as less toxicity and side effects [31–33]. In this study, we have evaluated the anticancer activity of Λ-Ru and Δ-Ru against different cancer cells: HeLa, HepG-2, SGC-7901 and A549 cell lines. MRC-5 cells, derived from human embryo lung fibroblast, were used as the control group. The conventional cytostatic agent cisplatin, a treatment for numerous malignances, was used as a positive control. Table 1 lists the IC_{50} values of Λ-Ru, Δ-Ru, cisplatin and other precursor compounds. Both Λ-Ru and Δ-Ru exhibited the broad spectrum of anticancer activity towards several types of tumor cells, with Λ-Ru showing greater performance. Λ-Ru showed a broad spectrum of inhibition on the tested cells (see Table 1) with IC50 values ranging from 7.6 ± 1.5 μM to 26.8 ± 3.6 μM, across the four types of cancer cell. Of note, was the treatment of SGC-7901 cells, in which Λ-Ru showed significantly lower IC_{50} values than those of Δ-Ru and other compounds, even cisplatin. The cytotoxicity of Λ-Ru was comparable or better than

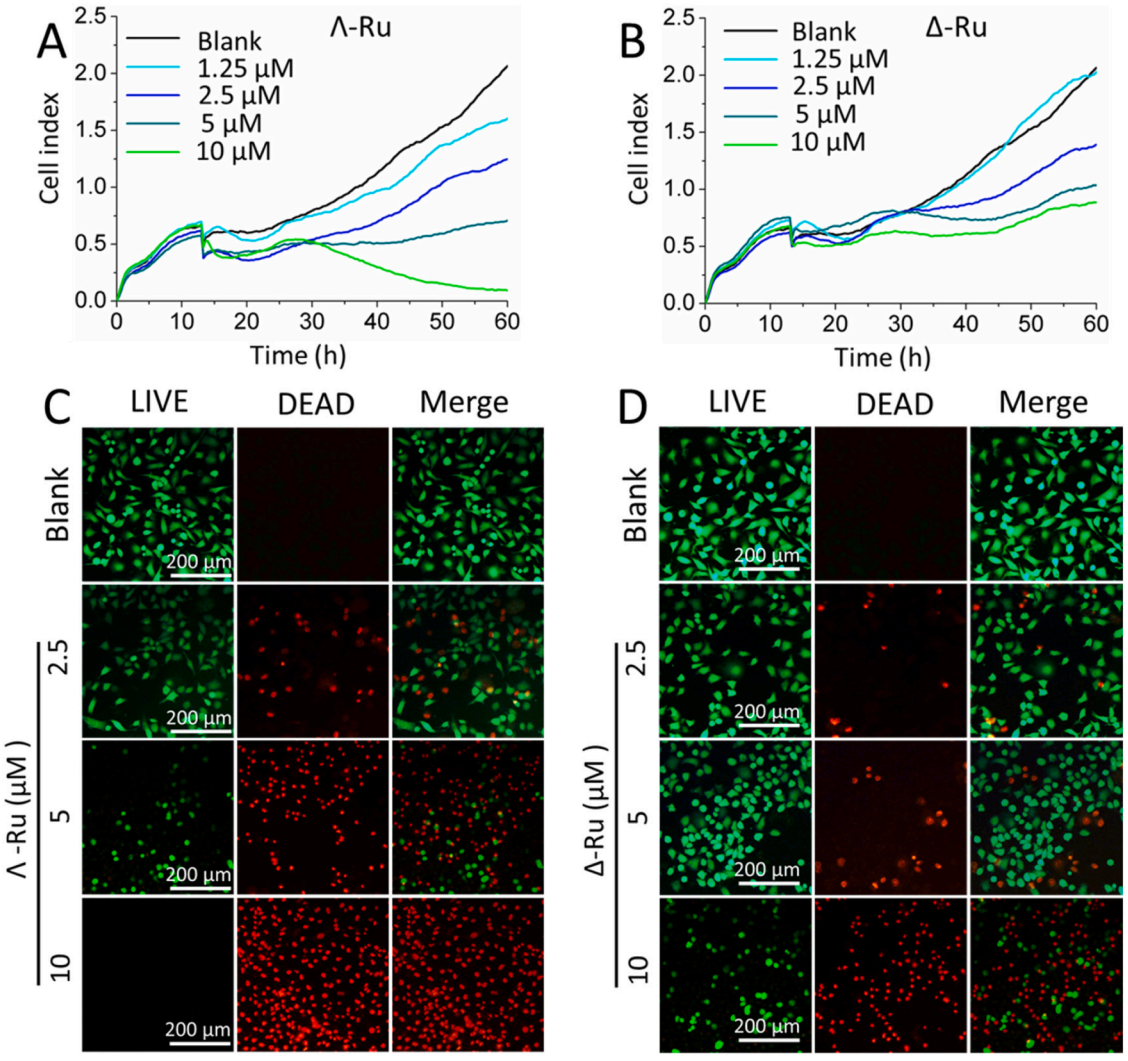

Fig. 2. Real-time visualizing of SGC-7901 cell proliferation effects of Λ-Ru (A) and Δ-Ru (B). After SGC-7901 cells were cultured for 12 h, the medium was removed, and a fresh medium with different concentrations of Λ-Ru and Δ-Ru (2.5 μM, 5 μM, and 10 μM) was added. SGC-7901 cells were incubated with the different concentration Λ-Ru and Δ-Ru for 12 h. After removing the culture medium, the SGC-7901 cells were co-stained by calcein-AM and PI for 30 min in the dark. Fluorescence microscopic images of Λ-Ru (C) and Δ-Ru (D) group were obtained through CLSM.

cisplatin for all the cell types except HeLa cells. Importantly, our control cell line, MRC-5 cells, showed lower toxicity of the Λ-Ru isomer, than the Δ-Ru isomer, and notably cisplatin (Λ-Ru 51.1 ± 3.1, Δ-Ru 36.3 ± 2.5 compared with cisplatin 36.8 ± 3.7 μM). The effect of Λ-Ru on cancer cell growth, showed a distinct preference for the SGC-7901 cells, indicating the higher cytotoxic effects towards these SGC-7901 cells as well as a good potency and low toxicity towards MRC-5 control cells.

To further investigate the obtained antitumor activity of Λ-Ru and Δ-Ru, the SGC-7901 cells were cultured with different concentrations of Λ-Ru and Δ-Ru. Adhesion and spreading were monitored by iCE-LLigence (Fig. 2A and B) [34–36]. The results are broadly similar to MTT analysis. Both could inhibit the proliferation of SGC-7901 cells with increase of concentration. Compared with Δ-Ru, Λ-Ru could better reduce the proliferation activity of SGC-7901 cells and result in cell death, even at low concentrations.

A fluorescence experiment was also conducted to investigate and verify the antitumor efficiency of Λ-Ru and Δ-Ru [37]. After treatment with Λ-Ru and Δ-Ru at different concentrations, the SGC-7901 cells were briefly stained using the LIVE/DEAD kit. The measurements are shown in Fig. 2C and D. The cells in the blank solution grew with a large cell body and clear cell membrane structures. However, the treated cells clearly exhibited morphological changes during apoptosis. With an increase in concentration, cells became increasingly round, the percentage of dead cells increased proportionally, and cell density decreased. These effects were particularly apparent in the Λ-Ru group.

To further evaluate the obtained anticancer activity, flow cytometric analysis was completed in which SGC-7901 cells were stained with Annexin V and propidium iodide (PI) after treated with Λ-Ru and Δ-Ru at different concentrations. Cells originally induced with Λ-Ru resulting in a high percentage of late-stage apoptosis, even at lower concentrations. With an increasing of concentration, this observation becomes more apparent. Fig. 3 shows the weaker apoptotic effect of Δ-Ru, compared with Λ-Ru, showing a slight increase in the number of cells in early and late apoptosis but no significant effect on cell cycle progression.

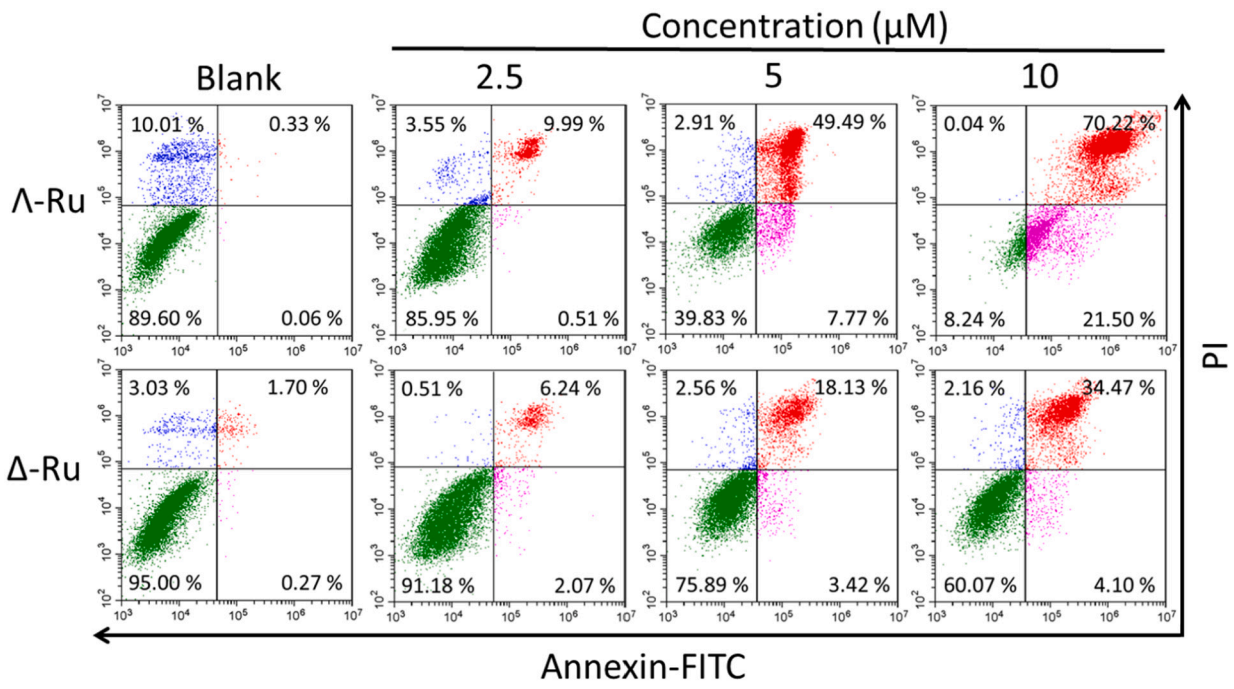

Fig. 3. SGC-7901 cells treated with Λ-Ru and Δ-Ru (2.5 μM, 5 μM, and 10 μM) for 12 h and analyzed using flow cytometry following Annexin V-FITC/PI staining. The blank group was PBS.

3.4. Cell integrity study

The result of fluorescence assay showed the survival rate of SGC-7901 cells after treatment. The cell morphology changes were observed by SEM and TEM. SEM could directly observe and study the surface morphology and other physical characteristics of cells without altering the cell shape in samples [37]. In the blank group (Fig. 4A), the cells had a plump cell morphology and long intercellular filaments. The cell surface was relatively uniform and smooth, and almost no cell debris were visible around the cells. In the treated group, the intercellular filaments were almost invisible, and the cells appeared shriveled. Specifically, the cell surface became broken in the 5 μM and 10 μM Λ-Ru treatment groups. The cell morphology changed considerably, and cell debris increased significantly. Simultaneously, regular cubes appeared on the cell surface, which might be Λ-Ru accumulated on the cell surface. Moreover, no remarkable changes were observed in the Δ-Ru group as the concentration increased. TEM was conducted to observe the internal structure of the cells and provide a reference for anticancer mechanisms [38]. The blank images of the SGC-7901 cells without exposure to Λ-Ru or Δ-Ru showed no significant changes in cell morphology and appeared to have clear cell walls. However, significant changes in the cell wall and internal structure could be observed after exposure to Λ-Ru and Δ-Ru. The cell walls particularly in the Λ-Ru group were disintegrated as concentration increased. The cytoplasm leaked, and the nuclear structure became unclear. Many cell fragments were observed around the cells and there were some hollow cells (Fig. 4B). These aforementioned results suggested that antitumor activity was related to compromised cell integrity and nuclear structure. Λ-Ru and Δ-Ru might have combined with DNA; hence these results.

3.5. Cell imaging

The obvious AIE-activity indicated that Λ-Ru and Δ-Ru exhibit potential as fluorescent agents for real-time cell imaging [39]. We stained the live SGC-7901 cells with Λ-Ru and Δ-Ru. The typical results of real-time fluorescence imaging of cells are shown in Fig. 5 and Fig. S5 (SI). The images revealed that the bright-red emission could be recorded when the cells were treated with Λ-Ru over time. The cells were not fluorescigenic initially; however, the fluorescence signal could be detected over time when the cells showed characteristics of apoptosis. The result of the aforementioned experiments indicated that Λ-Ru showed antiproliferative and real-time visualization activities (Fig. 5). Δ-Ru exhibited extremely low fluorescence intensity, which shows that it was difficult for it to target tumor cell nuclei (SI, Fig. S5). The reason for this needs to be explored in future experiments. The practical application of Λ-Ru as an effective probe for cell imaging should improve diagnostic analysis.

3.6. Cytotoxicity evaluation of Λ-Ru in vivo

The potential in vivo toxicity is often a significant concern for the clinical application of chemotherapy drugs [40]. To verify the applicability of Λ-Ru in vivo, the mice treated with different concentrations of Λ-Ru were evaluated. The mice showed slight and constant body weight gain 14 days after treatment under lower concentrations of 2.5 and 5 μM (Fig. 6A). Only the 10 μM group slightly decreased in weight. All mice were alive during the experiment under decreased concentration, and even in the 10 μM group, the survival rate remained at 83% (Fig. 6B). HE staining of organ sections (Fig. 6C) showed no sign of organ damage nor inflammation at the higher dose of 5 μM of Λ-Ru compared with the control group, indicating Λ-Ru has negligible side effects in vivo. The results indicate that Λ-Ru has negligible side effects in vivo. These observations have significant implications for the efficiency and safety of Λ-Ru in future clinical applications. A similar experiment using mice with tumors but treated with Δ-Ru (10 μM) was performed and also showed minimal side effects (SI, Fig. S6).

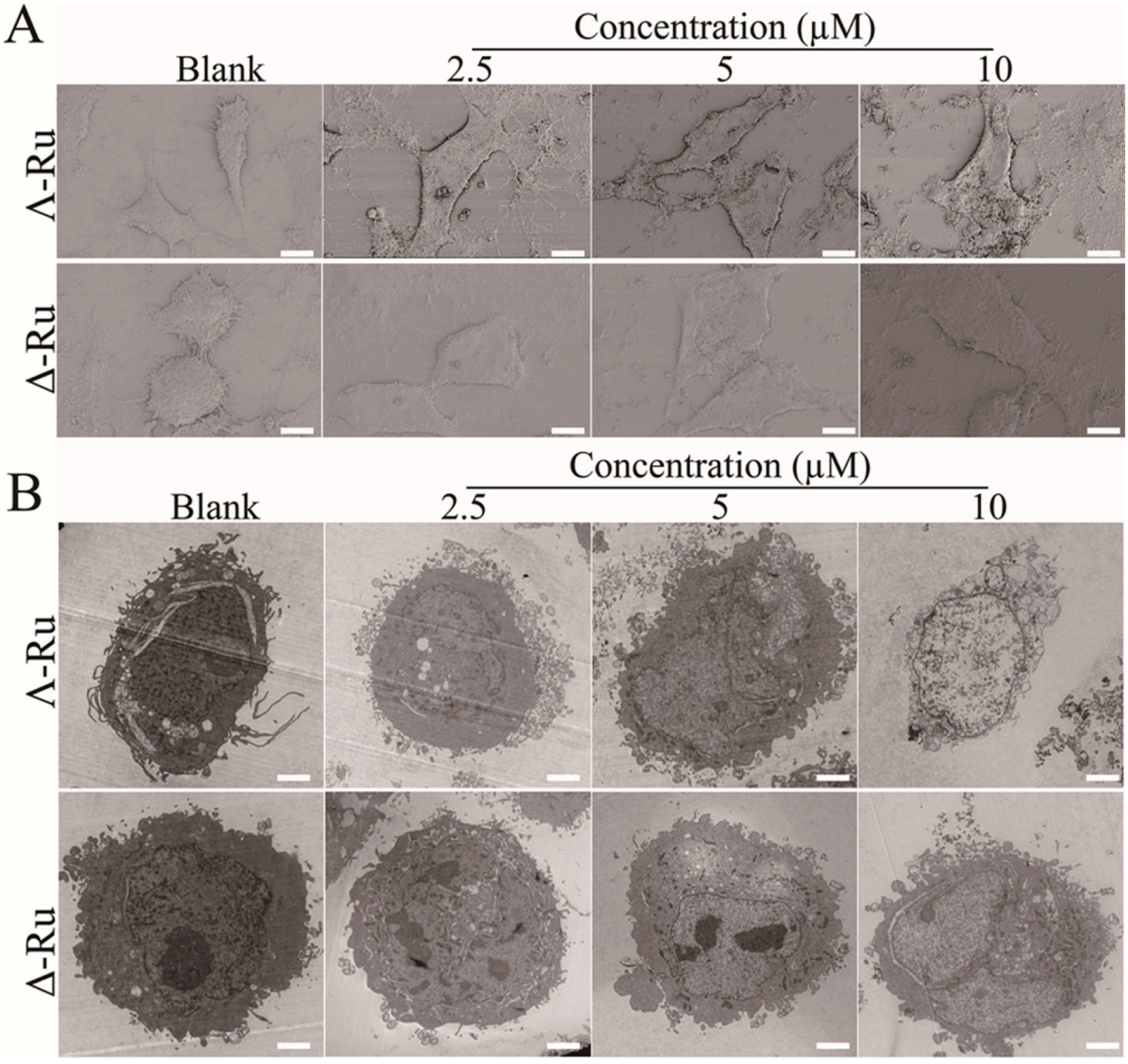

Fig. 4. (A) SEM images of SGC-7901 cells treated with different concentration of Λ-Ru and Δ-Ru (2.5 μM, 5 μM, and 10 μM) for 12 h. The blank group was PBS. Scale bar = 10 μm. (B) TEM images of SGC-7901 cells treated with different concentration of Λ-Ru and Δ-Ru (2.5 μM, 5 μM, and 10 μM) for 12 h. The blank group was PBS. Scale bar = 5 μm.

3.7. Λ-Ru inhibits tumor growth in subcutaneous SGC-7901 tumor bearing nude BALB/c mice

The in vivo antitumor activities of Λ-Ru were evaluated using an SGC-7901 tumor xenograft model. When the tumor mass reached a volume of approximately 100 mm^3, mice bearing the tumors were intravenously injected with either PBS, 2.5 μM Λ-Ru or 5 μM Λ-Ru. Comparison of the images of tumors (Fig. 7A) with those of the control group showed that mice treated with Λ-Ru markedly reduced the weight and size of the tumor. The tumor weight and size of the 2.5 μM group were less than those of the control group. However, the tumor weight of the 5 μM group was a half that of the control group. The tumor volume of the 2.5 μM group was only about a fifth of the control group. The relatively stronger antitumor effect in the 5 μM group suggests that Λ-Ru inhibits tumor growth in a dose-dependent manner. These results demonstrated that the administration of Λ-Ru inhibited tumor growth in xenograft mice models.

T_2-weighted magnetic resonance imaging (MRI) is increasingly being used by researchers to examine tissue lesion. The emergence of tissue edema could enhance the signal during treatment [41,42]. Thus, MRI was performed in the present study to examine the changes in tumor status. In Fig. 7B, an increase in the T_2-weighted signal indicates more apoptotic cell deaths with Λ-Ru treatment, and an increase in Λ-Ru concentration resulting in lower cancer cell densities within the tumor and a higher degree of tumor cell death. The 5 μM group also showed a smaller tumor volume.

In addition, the efficacy of treatment by Λ-Ru was assessed by histological analysis from different treatment groups 21 days after the treatments (SI, Fig. S7). Tumor growth curves of blank, 2.5 μM and 5 μM groups were collected. The results showed Λ-Ru treatment inhibited the growth of the tumor (Fig. 8A). Tumor weight of mice in blank, 2.5 μM and 5 μM groups after being treated for 21 days also showed a similar

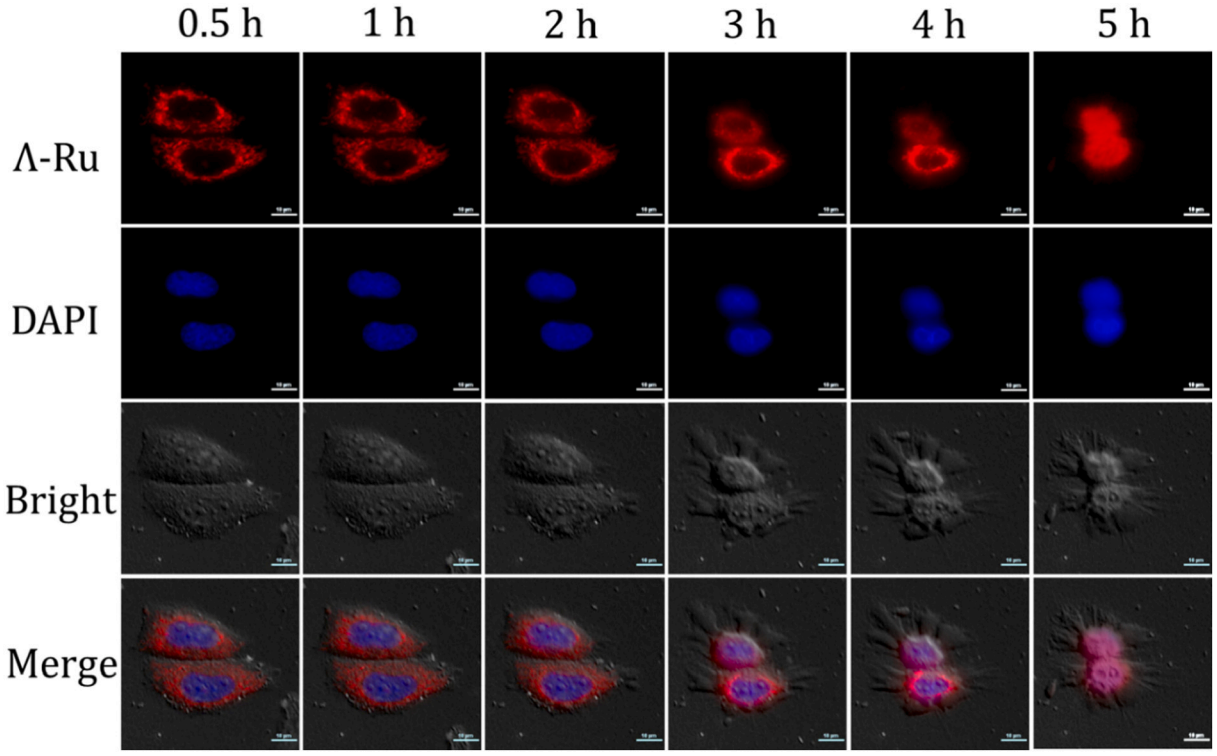

Fig. 5. Real time fluorescence imaging of SGC-7901 cells was induced by 5 μM Λ-Ru with a time from 0.5 to 5 h. All images share the same scale bar (10 μm).

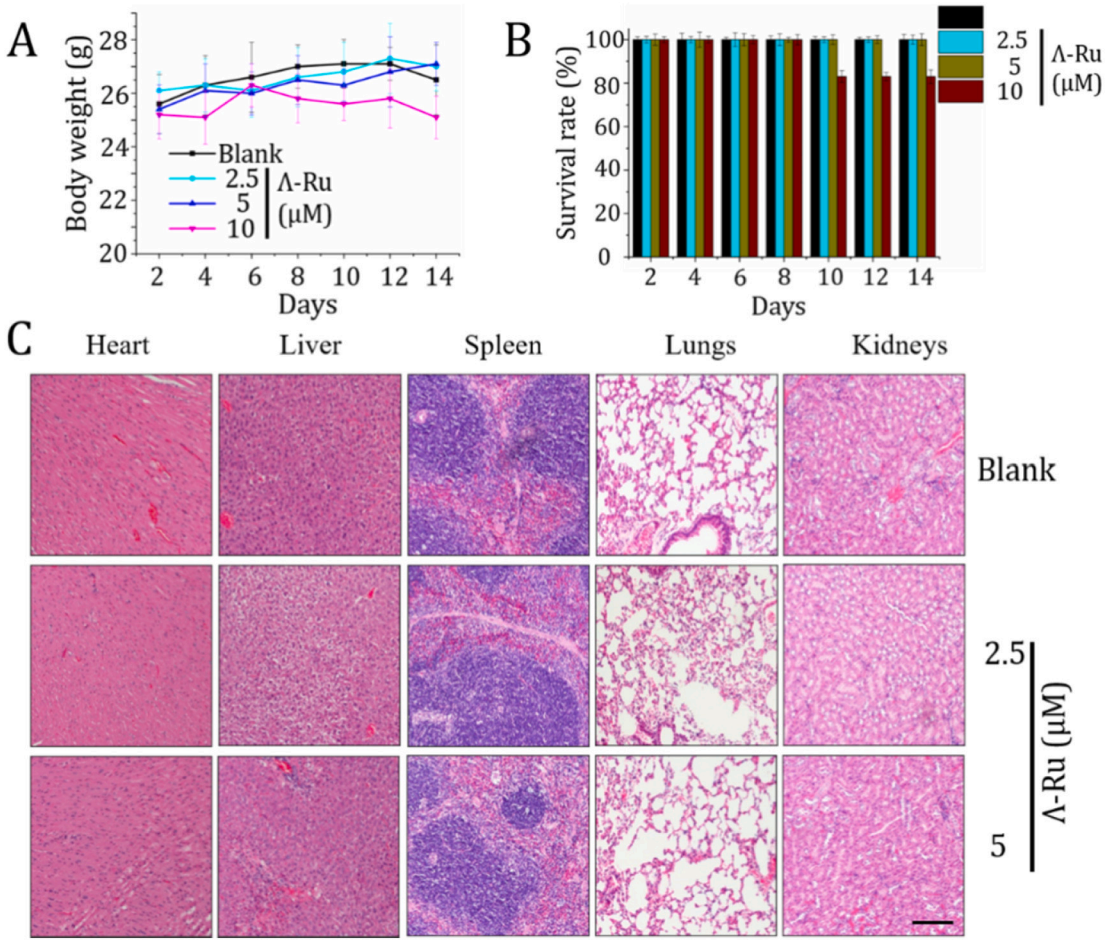

Fig. 6. (A) Body weight change line graph after treatments with different concentration Λ-Ru (2.5 μM, 5 μM, and 10 μM). (B) Survival rate histogram after treatments with different concentration Λ-Ru (2.5 μM, 5 μM, and 10 μM). (C) H&*E*-stained images of major organs. Each value represents the mean ± SD ($n = 6$). Scale bar is 200 μm.

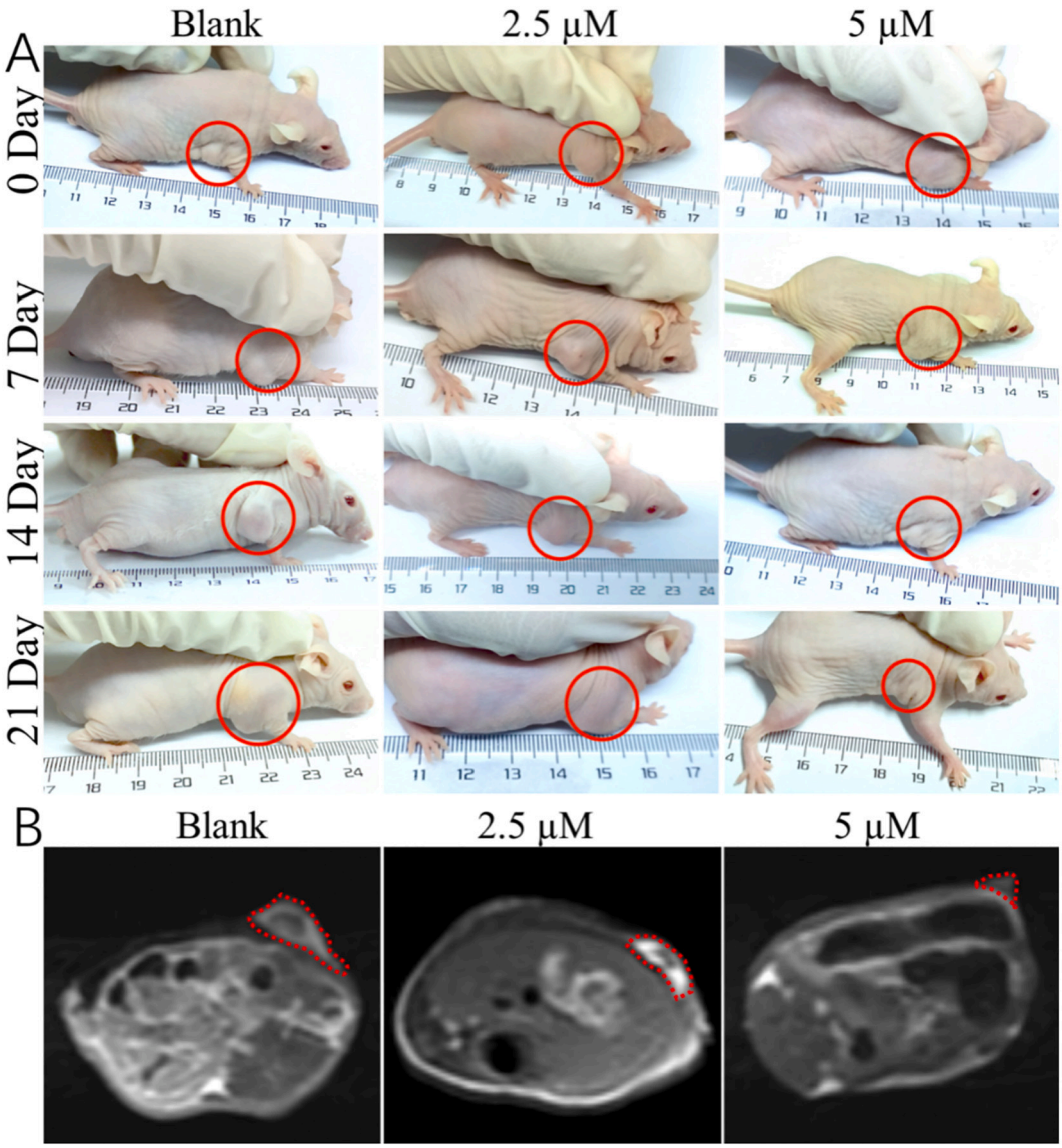

Fig. 7. In vivo applications of Λ-Ru on mice tumor xenograft. (A) Photographs of the mice taken in 7, 14 and 21 days of 2.5 μM and 5 μM Λ-Ru. (B)T_2-weighted MR images of SGC-7901 tumor-bearing mice after treated with 2.5 μM Λ-Ru and 5 μM Λ-Ru for 21 days.

result (Fig. 8B, and C). The tumor tissue is clearly damaged after the treatment. TUNEL–DAPI staining of the tumor section was used to evaluate cell apoptosis (Fig. 8D). DAPI could stain the cells with blue, and TUNEL could show the apoptosis cells as green. After the treatment with Λ-Ru, prominent necrosis was observed, indicating apoptotic cells. The mice treated with 5 μM Λ-Ru showed significantly lower tumor cellularity and more vacuolization, compared with the lower Λ-Ru concentration group, which is consistent with the observed dose-dependence. These results clearly suggest that Λ-Ru exhibits great potential for future cancer treatment.

3.8. Fluorescence image in vivo

Given the optical property of Λ-Ru and the aforementioned intracellular fluorescence imaging, Λ-Ru was further used to visualize cell apoptosis in living mice. An SGC-7901 tumor xenograft model was used in this experiment. The male nude SGC-7901 tumor-bearing BALB/c mice were anesthetized and injected with Λ-Ru (5 μM) via the caudal vein. The resulting fluorescence signal, shown in Fig. 9, does not appear prominent because Λ-Ru is not aggregated after injection. The fluorescence signal of the mouse was enhanced gradually over time and reached a maximum after 4 h. The fluorescence signal of the tumor in the mouse was significantly stronger than that from normal tissue. The result confirms that Λ-Ru can selectively detect and image SGC-7901 cells in vivo, and hence could visualize tumors.

4. Conclusion

In summary, we have prepared two new chiral ruthenium complexes (Λ-Ru and Δ-Ru) that exhibit AIE activity. These new diagnostic tools were prepared using a synthetic pathway that exploited ligands known to have AIE properties and ruthenium complexes with defined geometry and coordination chemistry. Despite the low solubility in water, both showed typical AIE characteristics and bound with duplex DNA from

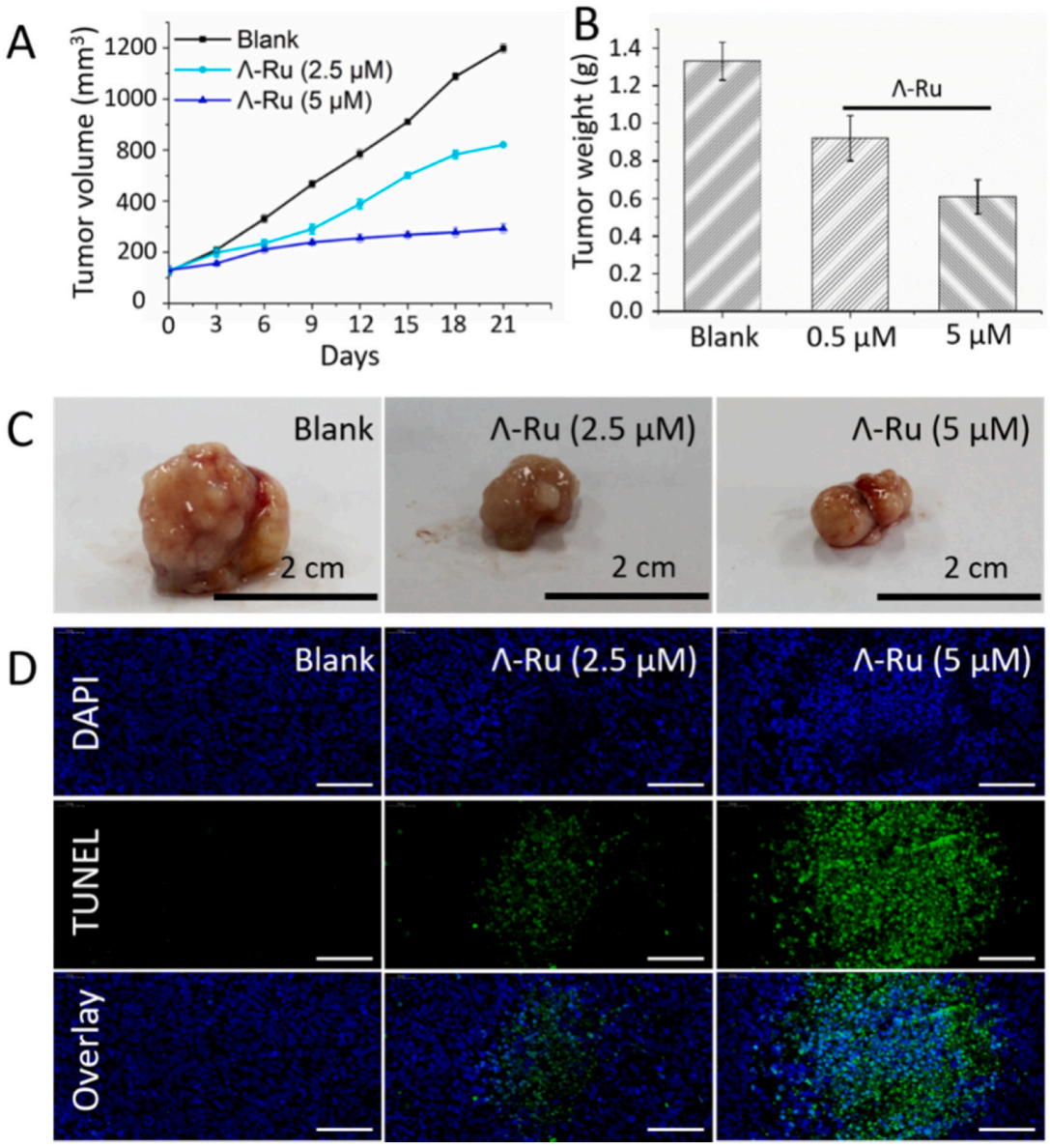

Fig. 8. Tumor tissue from SGC-7901 tumor-bearing BALB/c treated with PBS, 2.5 μM, and 5 μM Λ-Ru after 21 days. (A) Tumor growth curves. (B) Tumor weight. (C) Images of tumors stripped from the mice after 21 days. (D) Images of apoptotic cells of the tumor tissues following use of the TUNEL-DAPI technique. The scale bar is 100 μm.

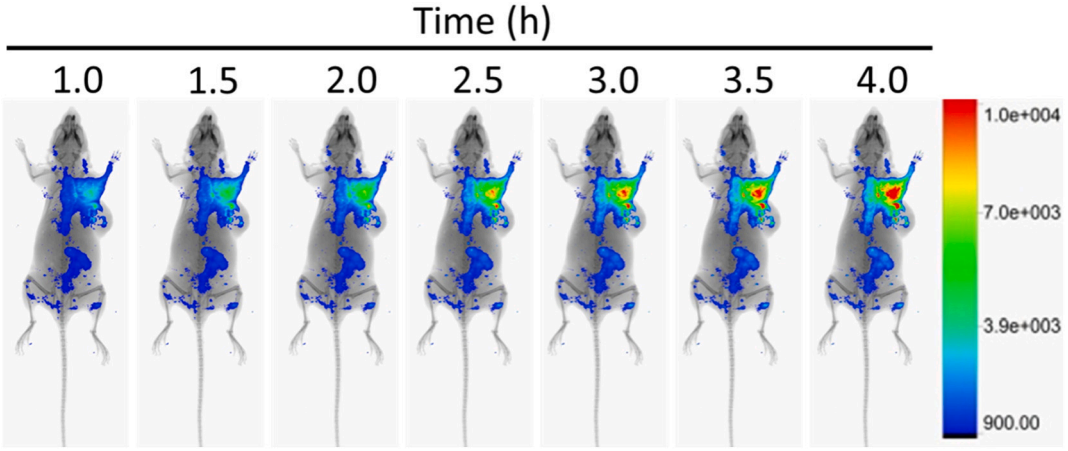

Fig. 9. Fluorescence images of SGC-7901 tumor-bearing mice after intravenous injection 5 μM Λ-Ru at different time points.

SGC-7901 cells, which was assessed by fluorescence intensity and viscosity data. In relation to antiproliferative potential, Λ-Ru was better than Δ-Ru in binding DNA from SGC-7901 cells. By using an SGC-7901 tumor xenograft mouse model, Λ-Ru was shown to inhibit tumor growth and real-time visualization. Thus, we conclude, that Λ-Ru provides an important advance in its capacity as a dual-function molecule for real-time visualization as well as a therapeutic agent towards SGC-7901 cells. These results not only provide important information about a design strategy for ruthenium complexes with AIE activity but also about a research tool for biological studies.

Declaration of Competing Interest

There are no conflicts to declare.

Acknowledgements

We would like to thank our colleagues from the biotechnology center of Anhui Agriculture University for their technical supports. This work was supported by the National Natural Science Foundation of China (21401002), the Natural Science Foundation of Anhui Province, China (1508085QB37), and as a Major Science and Technology Project of Anhui Province (17030701023). Financial support from the Australian Research Council (DP170103477) to L.L.M. is gratefully acknowledged.

Appendix A. Supplementary data

Supplementary data to this article can be found online at https://doi.org/10.1016/j.jinorgbio.2020.111339.

References

[1] W. Chen, R. Zheng, P.D. Baade, S. Zhang, H. Zeng, F. Bray, A. Jemal, X.Q. Yu, J. He, CA Cancer J. Clin. 66 (2016) 115–132.
[2] R.L. Siegel, S.A. Fedewa, K.D. Miller, A. Goding-Sauer, P.S. Pinheiro, D. Martinez-Tyson, A. Jemal, CA Cancer J. Clin. 65 (2015) 457–482.
[3] H. Chen, Z. Gu, H. An, C. Chen, J. Chen, R. Cui, Sci. China Chem. 61 (2018) 1503–1552.
[4] L. Chen, J. Wu, C. Schmuck, H. Tian, Chem. Commun. 50 (2014) 6443–6446.
[5] K. Horiguchi, S. Yoshikawa, A. Saito, S. Haddad, T. Ohta, K. Miyake, Y. Yamanishi, H. Karasuyama, Biochem. Bioph. Res. Co. 479 (2016) 517–522.
[6] K.N. Wang, X.J. Chao, B. Liu, D.J. Zhou, L. He, X.H. Zheng, Q. Cao, C.P. Tan, C. Zhang, Z.W. Mao, Chem. Commun. 54 (2018) 2635–2638.
[7] Y. Zhang, L. Pang, C. Ma, Q. Tu, R. Zhang, E. Saeed, A.E. Mahmoud, J. Wang, Anal. Chem. 86 (2014) 3092–3099.
[8] R. Zhang, Y. Yuan, J. Liang, R.T.K. Kwok, Q. Zhu, G. Feng, J. Geng, B.Z. Tang, B. Liu, ACS Appl. Mater. Interfaces 6 (2014) 14302–14310.
[9] G. Zhang, F. Hu, D. Zhang, Langmuir 31 (2015) 4593–4604.
[10] G. Wang, R. Zhang, C. Xu, R. Zhou, J. Dong, H. Bai, X. Zhan, ACS Appl. Mater. Interfaces 6 (2014) 11136–11141.
[11] Y. Hong, L. Meng, S. Chen, C.W. Leung, L.T. Da, M. Faisal, D.A. Silva, J. Liu, J. W. Lam, X. Huang, B.Z. Tang, J. Am. Chem. Soc. 134 (2012) 1680–1689.
[12] N. Zhao, S. Chen, Y. Hong, B.Z. Tang, Chem. Commun. 51 (2015) 13599–13602.
[13] V. Brabec, O. Nováková, Drug Resist. Updat. 9 (2006) 111–122.
[14] A. Bergamo, G. Sava, Dalton Trans. 13 (2007) 1267–1272.
[15] Q. Wu, K. Zheng, S. Liao, Y. Ding, Y. Li, W. Mei, Mini-Rev. Med. Chem. 35 (2016) 317.
[16] D. Sun, Y Liu, Q Yu, Y Zhou, R Zhang, X Chen, A Hong, J Liu, Biomaterials 34 (2013) 171–180.
[17] C.P. Popolin, M.R. Cominetti, Mini-Rev. Med. Chem. 17 (2017) 1435–1441.
[18] S. Masaoka, K. Sakai, Chem. Lett. 38 (2016) 182–183.
[19] A. Mitrović, J. Kljun, I. Sosič, S. Gobec, I. Turel, J. Kos, Dalton Trans. 45 (2016) 16913–16921.
[20] J. Diao, F. Bai, Y. Wang, Q. Han, X. Xu, H. Zhang, Q. Luo, Y. Wang, J. Inorg. Biochem. 191 (2019) 135–142.
[21] R. Hu, N.L. Leung, B.Z. Tang, Chem. Soc. Rev. 43 (2014) 4494–4562.
[22] D. Ding, K. Li, B. Liu, B.Z. Tang, Acc. Chem. Res. 46 (2013) 2441–2453.
[23] J. Mei, Y. Hong, J.W. Lam, A. Qin, Y. Tang, B.Z. Tang, Adv. Mater. 26 (2015) 5429–5479.
[24] W.Z. Yuan, Y. Gong, S. Chen, X.Y. Shen, J.W.Y. Lam, P. Lu, Y. Lu, Z. Wang, R. Hu, N. Xie, Chem. Mater. 24 (2012) 1518–1528.
[25] D. Sun, R. Zhang, F. Yuan, D. Liu, Y. Zhou, J. Liu, Dalton Trans. 41 (2012) 1734–1741.
[26] X. Chen, J.H. Wu, Y.W. Lai, R. Zhao, H. Chao, L.N. Ji, Dalton Trans. 42 (2013) 4386–4397.
[27] L. He, X. Chen, Z. Meng, J. Wang, K. Tian, T. Li, F. Shao, Chem. Commun. 52 (2016) 8095–8098.
[28] M. Banerjee, S.J. Emond, S.V. Lindeman, R. Rathore, J. Org. Chem. 72 (2007) 8054–8061.
[29] D. Sun, Y. Liu, D. Liu, R. Zhang, X. Yang, J. Liu, Chem. Eur. J. 18 (2012) 4285–4295.
[30] H.H. Gerets, K. Tilmant, B. Gerin, H. Chanteux, B.O. Depelchin, S. Dhalluin, F. A. Atienzar, Cell Biol. Toxicol. 28 (2012) 69–87.
[31] A.A. Almaqwashi, T. Paramanathan, P. Lincoln, I. Rouzina, F. Westerlund, M. C. Williams, Nucleic Acids Res. 42 (2014) 11634–11641.
[32] G. Süss-Fink, J. Organomet. Chem. 751 (2014) 2–19.
[33] H.J. Yu, L. Yu, Z.F. Hao, Y. Zhao, Spectrochim. Acta 124 (2014) 187–193.
[34] M. Roshan Moniri, A. Young, K. Reinheimer, J. Rayat, L.J. Dai, G.L. Warnock, Cytotechnology 67 (2015) 379–386.
[35] J. Sun, Y. Chen, Y. Wu, X. Zhang, L. Jiang, Y. Zhang, Chromatographia 78 (2015) 495–506.
[36] S. Ye, L. Jiang, J. Wu, C. Su, C. Huang, X. Liu, W. Shao, ACS Appl. Mater. Interfaces 10 (2018) 5862–5870.
[37] D. Sun, W. Zhang, Z. Mou, Y. Chen, F. Guo, E. Yang, W. Wang, ACS Appl. Mater. Interfaces 9 (2017) 10047–10060.
[38] L. Pan, J. Liu, Q. He, J. Shi, Adv. Mater. 26 (2014) 6742–6748.
[39] Z. Wang, Y. Gu, J. Liu, X. Cheng, J.Z. Sun, A. Qin, B.Z. Tang, J. Mater. Chem. B 6 (2018) 1279–1285.
[40] F. Hu, Y. Huang, G. Zhang, R. Zhao, H. Yang, D. Zhang, Anal. Chem. 86 (2014) 7987–7995.
[41] Y. Chang, L. He, Z. Li, L. Zeng, Z. Song, P. Li, L. Chan, Y. You, X.F. Yu, P.K. Chu, ACS Nano 11 (2017) 4848–4858.
[42] N.L. Leung, N. Xie, W. Yuan, Y. Liu, Q. Wu, Q. Peng, Q. Miao, J.W. Lam, B.Z. Tang, Chem. Eur. J. 20 (2014) 15349–15353.